IN-92
376554

Report on New Mission Concept Study: Stereo X-Ray Corona Imager Mission

P. C. Liewer[a], J. M. Davis[b], E. M. De Jong[a], G. Allen Gary[b], James A. Klimchuk[c], R. P. Reinert[d]

[a]Jet Propulsion Laboratory, MS 169-506, Pasadena, CA 91109
[b]NASA MSFC, Huntsville, AL 35812
[c]Naval Research Laboratory, Washington DC 20375
[d]Ball Aerospace & Technologies Corp., Boulder, CO 80306

Keywords: corona, space weather, stereoscopy, triangulation, spacecraft, high definition television, 3D visualization

ABSTRACT

Studies of the three-dimensional structure and dynamics of the solar corona have been severely limited by the constraint of single viewpoint observations. The Stereo X-Ray Coronal Imager (SXCI) mission will send a single instrument, an X-ray telescope, into deep space expressly to record stereoscopic images of the solar corona. The SXCI spacecraft will be inserted into a ~1 AU heliocentric orbit leading Earth by ~25° at the end of nine months. **The SXCI X-ray telescope forms one element of a stereo pair, the second element being an identical X-ray telescope in Earth orbit placed there as part of the NOAA GOES program.** X-ray emission is a powerful diagnostic of the corona and its magnetic fields, and three dimensional information on the coronal magnetic structure would be obtained by combining the data from the two X-ray telescopes. This information can be used to address the major solar physics questions of (1) what causes explosive coronal events such as coronal mass ejections (CMEs), eruptive flares and prominence eruptions and (2) what causes the transient heating of coronal loops. Stereoscopic views of the optically thin corona will resolve some ambiguities inherent in single line-of-sight observations. Triangulation gives 3D solar coordinates of features which can be seen in the simultaneous images from both telescopes. As part of this study, tools were developed for determining the 3D geometry of coronal features using triangulation. Advanced technologies for visualization and analysis of stereo images were tested. Results of mission and spacecraft studies are also reported.

1. INTRODUCTION

In 1996, NASA issued a call for proposals for studies of new mission concepts for space physics (NRA 96-OSS-03). One concept selected was a Stereo X-Ray Corona Imager (SXCI) mission and this paper summarizes the results of that study. The full report is available at http://spacephysics.jpl.nasa.gov/spacephysics/NewMissions.html.

The goal of the SXCI mission is to make the first stereoscopic observations of the X-ray corona in order to study, in three dimensions, the structure and dynamics of the corona and its magnetic fields. In this mission, a spacecraft carrying a single instrument, an X-ray telescope, is launched into a orbit at ~1 AU leading Earth by 25° after nine months. The soft X-ray telescope would be identical to the soft X-ray telescope that will already be in geosynchronous orbit on-board a NOAA GOES-series weather satellite and **the two instruments will be used together to form a stereo pair.**

This mission study includes the scientific rationale and goals and results for the mission and spacecraft design studies. A low-cost 420-day mission which samples a range of stereo angles was baselined and costed. In addition, studies were made of data analysis techniques and technologies for obtaining the necessary 3D information from only two simultaneous viewpoints. Several tools for this analysis were developed and tested on simulated stereo data created from solar rotation using both Yohkoh/SXT and SoHO/EIT data. These observations were also used to explore and develop advanced technologies for the display and analysis of stereoscopic data including 3D viewing of stereo images using liquid crystal shuttered goggles and stereoscopic High Definition Television (HDTV).

2. SCIENCE RATIONALE AND OBJECTIVES

Further author information: PCL Email: pauly@spaceport.jpl.nasa.gov; Telephone 818-354-6538

2.1 Objectives

The Earth travels through the extended atmosphere of a magnetically active star, our Sun. The Sun's outer atmosphere, the corona, is a dynamic million degree plasma extending outward from the 6000 K solar surface, the photosphere. The energy for heating the corona and solar wind is supplied by magnetic fields which are generated deep within the Sun by the solar dynamo and emerge through the photosphere. The buildup and release of magnetic energy in the corona is accompanied by changes in the three-dimensional structure of the corona and its magnetic fields which cannot be determined from single viewpoint observations. The uncertainties in interpreting the integrated single viewpoint line-of-sight observations of the optically thin corona are frequently so great that a significant understanding of the observed coronal structures and processes is not possible.

The most dramatic solar events are Coronal Mass Ejections (CMEs), prominence eruptions and solar flares. These explosive energy releases can cause geomagnetic storms and energetic particle events at Earth with harmful effects on spacecraft hardware, humans in space, communication and navigation systems, and electrical power grids. CMEs, the largest of the explosive events, are enormous (10^{15}-10^{16} g) bright masses of coronal material which move out from the Sun at up to 2000 km/s. They are thought to be the cause of the most severe space weather events, e.g., the largest geomagnetic storms and energetic particle events. The geomagnetic storms result when the CME impacts the Earth's magnetosphere. Solar flares also generate energetic particles which are a major factor in space weather. The most damaging particle events, however, are thought to be associated with interplanetary shocks driven by the fastest CMEs. Eruptive coronal events are generally thought to result from the release of energy stored in stressed coronal magnetic fields. To be able to predict these space weather events, one must understand the origin of these eruptive releases of magnetic energy in the corona.

The scientific objectives of this mission relate to the release of magnetic energy in the corona and require a determination of the three-dimensional structure of the corona and its magnetic fields and how these evolve in time. The two major objectives are

(1) What causes explosive coronal events such as CMEs, eruptive flares and prominence eruptions?

In spite of the importance of CMEs and other explosive events, there are major unanswered questions concerning the energy source (pure magnetic or partially gravitation?), the pre-event geometry (bipolar or quadrapole magnetic structure?; with or without flux rope?), and the role of reconnection, emerging flux, helicity and kink instabilities. The key to understanding the origin of CMEs and other eruptive events will be observations that allow us to determine in three-dimensions the structure and evolution of the corona and its magnetic fields before, during and after the events.

(2) What causes transient coronal loop heating?

The corona is completely filled with magnetic flux. It is not understood why only certain loops in the closed field regions of the corona are heated and filled with plasma while others are not. The heating may be caused by the dissipation of electric currents associated with magnetic stress (possibly involving magnetic reconnection and emerging flux), by the dissipation of MHD waves generated in the photosphere or low corona, by microflares and jets or by some combination of all. Determination of the 3-D geometry of the loop will allow us to constrain theories of loop heating and to relate the heating to photospheric phenomena, interactions with other magnetic flux systems, and structural changes in the loop.

Stereoscopic X-ray data are essential to obtaining the necessary 3-D information on the structure and dynamics of the corona needed for these objectives. The corona is a million degree plasma that radiates strongly in X-rays, the intensity of the emission being proportional to the square of the plasma density. However, since the magnetic field pressure in the corona is generally greater than the plasma pressure, the magnetic field restricts the motion of the plasma, forcing it to follow the magnetic field lines. Since only magnetic field lines which hold hot ($>10^6$ K) plasma radiate, the X-ray emission directly traces those coronal magnetic field lines with heated plasma.

Many questions relating to the science objectives can answered with the stereo X-ray observations alone (Table I). For maximum scientific benefit, the stereo X-ray data can be supplemented with other solar observations as available from ground based observatories and spacecraft such as SoHO or Solar B. Specifically, supplementing the X-ray observations with magnetic models of the corona extrapolated from magnetograms will considerably enhance our understanding of the 3D evolution of the coronal magnetic fields and the energy stored in them. The fraction of the total magnetic energy that is available to heat the corona and to power dynamic phenomena is stored in the component of the field that determines the coronal currents, the non-potential component. Using force-free magnetic field models (Ref. 1 and references therein)

computed from daily vector magnetograms and constrained by the stereo observations will allow us to quantify the non-potential component of the magnetic field and show how the stored energy builds up with time and how it is released (in transient or eruptive events) or how it decays. Scientific objectives which can be achieved using both X-ray and vector magnetogram data are described in Table I.

The primary mission of this study lasts 460 days and covers stereo angles in the range 0-25°; this was determined to be sufficient to meet the above major scientific objectives as well as specific objectives. However, the orbit chosen for this study was a drifting (not fixed angle) orbit such that by 18 months, a separation of 50° is reached. At these larger separation angles, additional scientific objectives can also be achieved (Table I).

Table I. Scientific Objectives

Major Scientific Objectives

- Determine the cause of explosive coronal events such as coronal mass ejections (CMEs), eruptive flares and prominence eruptions.

- Determine the cause of transient coronal loop heating.

Specific Objectives from Stereo X-ray Data Alone (0-40° Stereo Angle)

- Determine definitively if there are interacting coronal loops causing loop heating. The stereo observations will identify unambiguous points of enhanced emission and determine whether the emission is due to enhanced heating/density or line-of-sight effects.

  Determine the three-dimensional geometry of coronal structures, e.g., loops, coronal hole walls, helmet streamers and CMEs. From time sequences, determine the speeds and direction of motion of features that can be identified in both images. Use to analyze the 3D evolution of the corona during eruptive events as well as transient loop heating.

- Determine the photospheric footpoints of coronal loops by downward extrapolation. Study the importance of photospheric velocity, photospheric magnetic fields and flux emergence to heating coronal loops.

- Study the role of the dark cavity in CMEs and consequently the possible role of magnetic buoyancy and gravity in CME initiation. Lack of a dark cavity in single viewpoint observation of a pre-CME configuration may be a line-of-sight effect.

- For CMEs viewed along the arcade axis, look for closed field lines around the CMEs to determine if reconnection in the low corona precedes CME initiation. Theories vary as to whether reconnection proceeds or follows CME lift-off and whether the reconnection occurs low in the corona (below the flux rope) or higher in the corona (above the arcade

Specific Objectives from Stereo X-ray Data plus Magnetic Field Models (0-40° Stereo Angle)

- Determine the 4D (3 spatial dimensions plus time) evolution of the magnetic field configuration accompanying eruptive events and heating using force-free models of the coronal magnetic fields with measured photospheric fields as boundary conditions. Specifically, quantitatively analyze roles of photospheric velocity shear, and flux emergence in CME initiation. Use to constrain theoretical models of such.

- Determine the non-potential component of the field to determine energy build up and release accompanying eruptive events and heating using force-free models of the coronal magnetic fields with measured photospheric fields as boundary conditions. Use to constrain theoretical models of such events. Determine deviations from force-free fields indicating role of pressure and/or gravity.

- Determine the photospheric footpoints of coronal loops by identifying field lines in stereo observations with field lines in magnetic field models. Analyze the importance of photospheric velocity, photospheric magnetic fields and flux emergence to heating coronal loops.

Specific Scientific Objectives for Extended Mission (>40° Stereo Angle)

- Study evolution of coronal features for longer time scales made possible by extended longitudinal X-ray coverage of Sun provided by the two X-ray telescopes.
- Study evolution of X-ray corona for regions of Sun underlying CMEs seen on the limb from near-Earth coronagraphs.

2.2. Limitations of a single viewpoint and the need for stereo observations

The X-ray and EUV images from the Yohkoh and SoHO missions have provided many exciting results on the structure and dynamics of the solar corona. However, like all single vantage point observations, the images are often ambiguous in their interpretation.

Understanding both a coronal loop's geometry and the photospheric location of its footpoints is important for understanding the loop's heating and its relationship to photospheric phenomena. Single viewpoint observations of an isolated coronal loop are insufficient to determine the 3D loop geometry because the angle that the loop makes with respect to the plane of the sky is not known. One cannot extrapolate a loop reliably from the point it disappears in the lower corona to the photosphere unless the angle with respect to the plane of the sky is known.

Interpretation of single line-of-sight observations is further complicated by the fact that the coronal structures are optically thin at X-ray/EUV wavelengths. Coronal loops, and the larger structures that they comprise, are not in general isolated. Other structures often lie along the line-of-sight, either in front of or behind the structure of interest causing a "background" problem. With only a single viewpoint, it is often difficult, if not impossible, to disentangle the various structures that overlap along a single line-of-sight within an image. Many Yohkoh images show loops apparently interacting with adjacent loops. But without a stereo view point, it is not possible to resolve the ambiguity of whether the brightenings of the loops are a result of summing intensities along the line of sight or if the loops physically interact. It has been demonstrated that the ambiguities associated with unknown line-of-sight effects can have a sizable impact on the interpretation of Yokoh data.[2,3] Stereo observations will eliminate these ambiguities and allow for a much more accurate determination of loop densities and pressures. We will thus be able to investigate the detailed variations of temperature, density, and pressure along the axes of loops, which will give us a much better understanding of loop heating and dynamics.

In some eruptive event scenarios, the energy release is triggered by the interaction of neighboring flux systems. But a close neighbor in a 2-D view may be quite distant when the third dimension is considered. Thus it is essential to have the stereo observations of the X-ray/EUV corona to resolve such ambiguities in the interpretation of changes in the coronal structure.

Most theories of the origin of eruptive events including CMEs and eruptive prominences involve changes in the three-dimensional geometry of the corona which can not be determined from single view point observations. For example, several theories involve arcades overlying filaments and filament channels. A dark cavity may surround the filament, but lack of a dark cavity in a single viewpoint observation may be a purely line-of-sight effect. A build up of magnetic energy from photospheric flows, flux emergence, reconnection below the filament or magnetic buoyancy may cause the eruption. In some arcade models, the arcade footpoints are sheared resulting in an expansion of the loops; eruption results when some critical shear level is reached.[4] In other scenarios, the field is stressed by converging photospheric flows which bring opposite polarity fields to the neutral line whereupon they reconnect. A coronal flux rope or filament, created by the reconnection, steadily grows with time. In some circumstances a loss of equilibrium may eventually occur and this could result in a full eruption.[5] In other scenarios, interaction of the arcade-prominence system with an emerging flux system is responsible for the eruption[6] or a pre-event quadrapole magnetic geometry make be the key.[7] A kink instability[8,9] or reconnection between existing loops[10] are also candidates for triggering the eruptive event. Clearly, single view point line-of-sight observations do not give us enough information about the evolution of the coronal fields to distinguish between various models.

3. DETERMINING THE 3D STRUCTURE OF CORONAL FEATURES USING TRIANGULATION FROM STEREO PAIRS

It has not been generally appreciated that quantitative information on the 3D magnetic fields can be found by using "triangulation" of coronal loops and other structures observed from two simultaneous views (i.e., from two spacecraft). Using classic surveying techniques, the solar coordinates in *three-dimensions* of a coronal "feature" can be determined from only two simultaneous views as long as (a) one knows the angular separation of the two views and the spacecraft-Sun distances and directions and (b) one can recognize the "feature" in both images. This technique was used on Skylab loops[11] and on simulated loops[12]. The use of triangulation to determine the 3D magnetic structure from two views is limited to structures and features easily identified in both images and this can be a serious limitation. For features which can be identified, this technique can be used to trace out the feature, and thus the magnetic field lines, in three-dimensions.

The triangulation technique for a simple case is shown schematically in Fig. 1 where, for simplicity, it is assumed that both views are from the equatorial plane of the Sun. In this figure, the coordinates in the plane of the sky of the two views with stereo angle α are related by the simple rotational transform

$$T(\alpha) = \begin{pmatrix} \cos\alpha & \sin\alpha & 0 \\ -\sin\alpha & \cos\alpha & 0 \\ 0 & 0 & 1 \end{pmatrix}.$$

As part of this study, we have developed analysis tools which use triangulation to determine the 3D coordinates of coronal features and structures. These tools have been developed using simulated stereo pairs formed using solar rotation and tested on true stereo pairs made using simple known loops. With the tools, the user identifies and marks the location of the same coronal feature in both images of a stereo pair. The two points located in this way are called "tiepoints." The pair of (i,j) coordinates (in pixels) of the feature tiepoints are put in a "tiepoint" file. A program called XYZSUN computes the 3D solar coordinates of the tiepointed features from the tiepoints. These tools have been developed for the general case where the solar rotation axis is at an arbitrary angle with respect to the optical axis. In this general case, the transformation matrix involved becomes more complicated than the simple single-axis rotation matrix *T(α)* shown above.

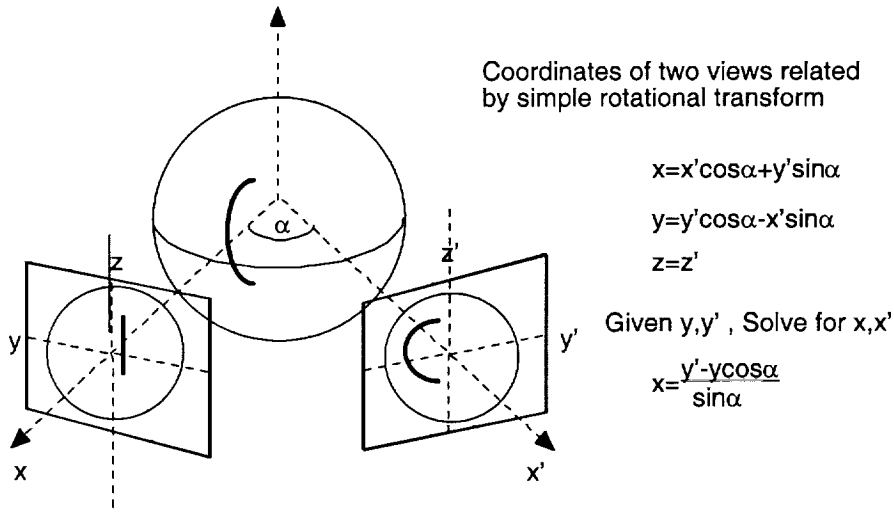

Fig. 1. Determination of coronal loop height via triangulation. Coronal loop as seen from two view points separated in the ecliptic by stereo angle α. The coordinates in the plane of the sky for the two views are related by a simple rotational transform and the complete 3D geometry of the loop can be determined from the measured (x,y) and (x',y') as shown.

The code XYZSUN, which takes the tiepoints and uses triangulation to compute the 3D location of the features in solar coordinates (Solar radius, latitude and longitude), uses user inputs and the JPL NAIF-SPICE solar system ephemeris. XYZSUN works by first determining the coordinate transformation between the telescope/camera frame of reference and the solar coordinate system.[13] Let P=(x,y,z) be the location of a point in the solar coordinate system (centered on the Sun) and let P'=(x',y',z') be the same point in the telescope/camera coordinate system with the z' axis along the optical axis and the x'-y' plane parallel to the image plane (located at z' = -f where f is the focal length). The transformation between P and P' can be written as the sum of a rotation plus translation:

$$\boldsymbol{P'} = \boldsymbol{M}\,\boldsymbol{P} + \boldsymbol{R}_{s/c}$$

where $\boldsymbol{M}$ is a full 3x3 rotational transformation matrix and $\boldsymbol{R}_{s/c}$ is the vector from the center of the camera system to the center of the Sun. This is the transformation used by XYZSUN. XYZSUN currently assumes that the spacecraft is in Earth-orbit since at present we have only rotational stereo data, but can be easily modified to use the spacecraft orbits for a stereo mission. Using the time at which each image was taken, XYZSUN uses the ephemeris data to determine the solar longitude and latitude of the sub-solar point of the spacecraft and the distance from the Sun to the spacecraft. XYZSUN also needs information on the telescope focal length f and the location of the optical axis on the image (in pixels) to be able to transform between image coordinates (pixels) and camera and solar coordinates. Using the above, the tiepoint from each image of a pair determines a ray tracing backwards from the image plane towards the Sun. If there were no errors, the two rays would

intersect at the location of the tiepointed feature. However, errors are introduced by the spacecraft, the telescope and the tiepointing itself. Therefore XYZSUN actually computes the point of closest approach (in solar coordinates) of the two rays and the location of the feature is taken to be midway between the two rays at closest approach. The program also has a manual "test" mode for use with simulated data or with data where ephemeris and/or focal length data are not available and this mode was used to test the code on simple 3D loops with known coordinates. A stereo image pair was created by rendering images of the loops from two angles separated by 15°; this image pair is shown in Fig. 2. A tiepoint file of points lying on these loops was created using the `3DCursor` tool and the 3D coordinates of these points were then computed by XYZSUN and compared with the known coordinates. Shown on the right in Fig. 2 are the (x,y,z) location of points (X's) determined in this way plotted over the known test loops (solid lines); agreement is excellent.

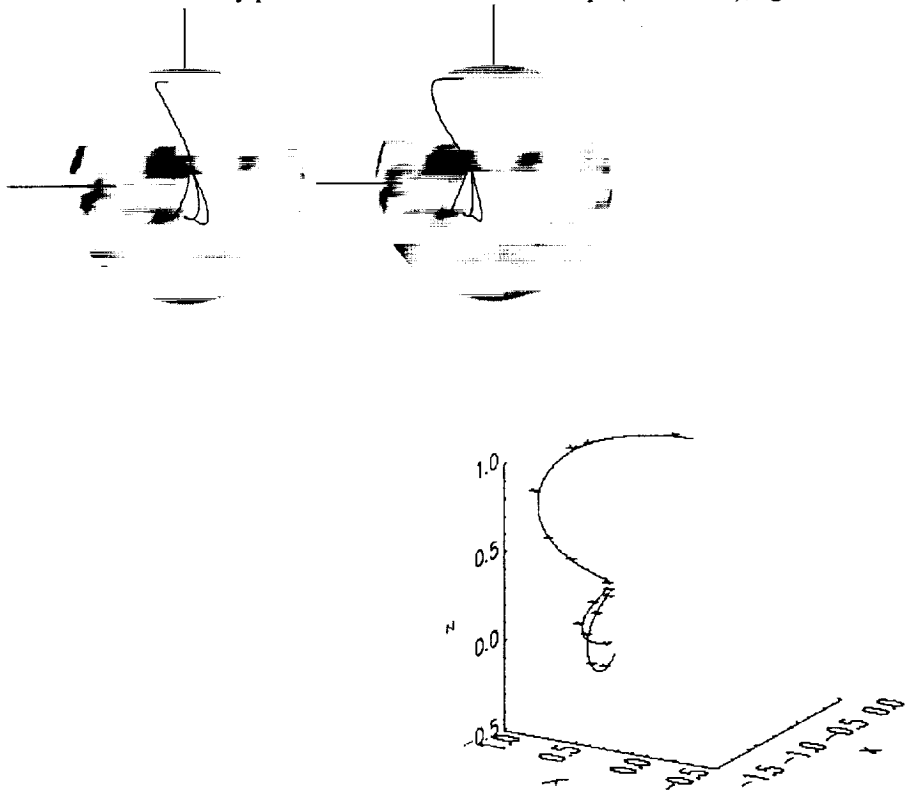

Test Loops Tiepointing Results (X)

Fig. 2. Test of determination of 3D loop geometry on known loops. The test stereo image pair (top) was created by viewing the known loops from two angles separated by 15° (This pair may be viewed in stereo by relaxing your eye focus). The (x,y,z) location of points (X's) determined by triangulation from the stereo pair are plotted over the known test loops (solid curves). Agreement is excellent.

Two tools were developed during this study to create tiepoints between stereo image pairs. The first method for creating uses the commercial software package ENVI which runs under IDL. The user views the two images of the stereo pair in side-by-side windows and locates the same features in each image using cross-hairs. When the user has located the same feature in each image, the software adds the pixel coordinates of the two tiepoints points to a tiepoint file.

The second tool for tiepointing, called the `3DCursor`, utilizes true stereoscopic "three-dimensional" visualization on Silicon Graphics workstations which support stereo visualization using an interlaced screen and electronically shuttered goggles (see Sec. 4). The liquid crystal goggles shutter between left and right eyes coherently with the screen sweeping the left and right eye images so that each eye sees only one image and the user sees the image in stereo 3D. Using the `3DCursor` tool, the user can move a tiepoint in all three dimensions, placing it on features as seen in his 3D stereo view. Thus as he moves the cursor in the z-direction (perpendicular to the screen), the cursor and tiepoint seem to move in and out of the Sun. In reality, the separation of the tiepoint location on the left and right eye images is changing, making the cursor appear to move in and out in the stereo view. Once the cursor is located on a feature, the user adds this tiepoint to a tiepoint file. Since the

3DCursor program is actually moving two tiepoints, one in the right eye image and one in the left eye image, this tool determines the pixel coordinates of a feature in both images just as does the first tool. Tiepoint files created using ENVI can also be read into the 3DCursor tool (and vice versa) and viewed in stereo.

Various sources of error contribute to uncertainties in the solar coordinates of a feature computed from the tiepoints. Errors in placing the tiepoints, in the alignment of the images, in the location of the optical axis on the image and in the vector from the spacecraft to the Sun center will all contribute to errors in the final solar coordinates. The accuracy also depends strongly on both the resolution of the image itself and the stereo angle. Referring to Fig. 1, alignment, tiepoint placement and resolution would contribute to errors in determining the coordinates (y,z) and (y',z'); call this error Δy. The error introduced into the determination of the coordinate in the third direction (x, x' in Fig. 1) by the error Δy depends on the stereo angle via the transformation. This error is $\Delta x \sim \Delta y/\sin\alpha$ where we have used the simplified transformation $x=(y'-y\cos\alpha)/\sin\alpha$ (Fig. 1). This shows that the overall error in determining the 3D coordinates of a feature is larger than the error in locating the tiepoints by $1/\sin\alpha$ and thus reasonably large stereo angles are needed for accurate 3D coordinate determination. For example, a stereo angle of 15° leads to a multiplication of the error Δx by $1/\sin\alpha = 3.9$ increasing the overall error in the 3D location of the feature by this factor. A one pixel error in locating a tiepoint on a 1024x1024 solar image gives an error $\Delta y/R_S = 0.25\%$ assuming the solar radius is 400 pixels and thus the overall error is increased to $\Delta R/R_S \approx 1\%$ or 7000 km.

The above error analysis suggests that the optimum angles would have $\sin\alpha \approx 1$. However, the most serious source of error is most likely to be the ability to identify same feature accurately in both images of the stereo pair due to differences in the appearance of the "feature" in the two images or due to the fuzziness of the feature itself and this fact argues for smaller stereo angles. In rotational stereo pairs, the actual changes in the corona mean that the same feature may not even be present in both images or it may have changed location. For true stereo images, the fact that the corona is optically thin in X-rays will cause differences in a feature seen in two simultaneous images. The ability to identify and tiepoint the same feature in both images is a serious limitation of this technique and feature identification is easier for smaller stereo angles. Therefore, stereo angles in the range of 15-30° are probably optimum for analyzing the coronal structure via triangulation of features. A study[12] using simulated stereo X-ray data of loop complexes determined that the optimum angular separation was approximately 30°.

4. ADVANCED TECHNOLOGIES FOR VISUALIZATION AND ANALYSIS OF SOLAR IMAGES

4.1 Use of standard computer monitors for 4D display of stereo image pairs

The use of advanced digital technologies for the display and analysis of stereo X-ray image sequences will greatly enhance the science return from stereo missions. The human brain has adapted to extract the three-dimensional (3D) structure of objects from two-dimensional (2D) stereo image pairs. Humans can extrapolate 4D object motion and structural changes from a small sequence of images. We perceive the world through two closely spaced optical sensors which form sequences of 2D images on our retinas. A complex neural network processes these sequences to create a 4D model of our universe. This process "automatically" recognizes, classifies and separates differences in the 2D patterns. It identifies which patterns are associated with temporal and spatial changes and modifies the model accordingly. The process must properly identify whether the pattern changes are associated with object motion, structural changes, changes of viewpoint, or lighting changes.

The human visualization capability can be utilized for the analysis of the 4D structure of the corona. In Sec. 3.A, we discussed the use of one new technology for the 3D presentation of stereo data: Silicon Graphics computer monitors equipped with synchronized liquid crystal shuttered glasses enable users to view stereo images. The stereo pair is displayed as two separate (odd-even) "interlaced fields." The left eye (odd lines) and right eye (even line) fields are displayed alternately at 60 Hz. The viewer wears 60 Hz liquid-crystal shuttered glasses which opaque the left and right eye alternately in synchronization with the alternating fields displayed on the monitor. This technology was used to implement the 3D cursor tool for triangulation described in Sec. 3.A. A time sequence of stereo pairs, may be examined in the same way thus enabling the evolution of coronal features to be studied. Shuttered-liquid crystal technology will soon be inexpensive and widely available because of its application to the computer gaming industry.

Table II. Comparison of Technologies for 3D & 4D Stereo Visualization

Device	Resolution (eyes-x-y)	Images per sec	Comments
Standard TV interlaced	1x640x480	30	data storage (video tape) analog and lossy; not suitable for archiving
Standard TV	2x640x240	60	interlaced left&right eye (odd/even lines); stereo using

stereo interlaced			60 Hz synchronized electronically shuttered goggles;
Standard Computer monitor (non-interlaced)	1x1024x768	60	data storage is digital
Standard Computer monitor (stereo interlaced)	2x1024x384	60	interlaced left&right eye (odd/even lines) stereo using 60 Hz electronically shuttered goggles; data storage is digital
US HDTV Computer Monitor (non-interlaced)	1x1920x1080	60	data storage digital; suitable for archiving. (Also digital tape decks using 1/2" digital tape)
US HDTV stereo interlaced	2x1920x540	60	interlaced left & right eye; stereo using 60 Hz electronically shuttered goggles;
US HDTV stereo non-interlaced	2x1920x1080	120	polarized glasses & screen filter (120Hz synchronized); digital data storage; suitable for archiving.

It should be noted that the vertical resolution of "stereo interlaced" images is one-half of "non-interlaced monoscopic" images using the same display device. The horizontal resolution is unaffected. For example, a standard SGI computer monitor has a resolution of 1024 pixels horizontally and 768 pixels vertically when used to display non-interlaced monoscopic images. When used in interlaced stereo mode, only half of the lines are available for each image and thus each image is 1024x384 which is inadequate for the display of 1024x1024 image pairs (or even 512x512 images). Standard computer monitors are compared to both standard TV and high definition TV monitors in Table II. Note that standard TV can also be used in interlaced stereo mode. However the low resolution (640x240) coupled with the lossy data storage medium (NTSC analog video tape) make this an unattractive option. New Digital Television (DTV) equipment will provide additional options in the future. The same computer technology can also be used to project stereo image sequences and stereo animations on a large projection screen.

4.2. Use of stereo High Definition Television (HDTV) computer monitors

High Definition Television (HDTV) provides significantly higher resolution than standard computer monitors. An HDTV monitor built to the US industry digital "standards" has 1920 pixels horizontally and 1080 pixels vertically. Japanese monitors have 1920 pixels horizontally and 1035 pixels vertically. Data can be stored on any digital medium, including 1/2" digital tape. The cost of HDTV equipment will decrease dramatically as HDTV is broadcast into homes in the US. HDTV can be used for stereo viewing by interlacing left and right eye images and viewing the monitor with 60 Hz synchronized liquid-crystal goggles as described above for standard computer monitors. In this case, each images is 1920x540 which is an improvement over the 1024x384 for standard monitors. This technology was used in this study to create a stereo HDTV video using "rotational" stereo data from SXT and EIT. JPL has a small demonstration room equipped with a Electrohome projector which can display an HDTV video on a sixteen by nine foot screen in stereo to a group with each person wearing 60 Hz synchronized shuttered-goggles.

HDTV stereo images can also be displayed in a non-interlaced mode. This option provides the highest available broadcast resolution (last option shown in Table II). The left and right eye images are displayed at full resolution (1920x1080) *alternately in time* with a frequency of 120 Hz. Stereo viewing is accomplished by using 120 Hz synchronized liquid crystal shuttered glasses or placing a polarizing screen in front of the HDTV monitor which alternates the transmitted polarization at 120 Hz synchronously with the HDTV monitor display. In the latter case, the viewer wears only inexpensive polarized glasses. This technology was not explored in this study.

5. MISSION DESIGN, STEREO ANGLE AND ORBIT

The Stereo X-Ray Corona Imaging (SXCI) Mission requires the launch of a single spacecraft with a soft X-ray imaging (SXI) instrument into an approximately 1 AU orbit in the ecliptic plane leading or lagging Earth. The SXI would be identical to the instrument that will be in geosynchronous orbit on-board a NOAA GOES-series satellite and the two instruments would be used as a stereo pair. The GOES (Geostationary Operational Environmental Satellite) spacecraft are a continuing series of NOAA weather satellites aimed primarily at forecasting terrestrial weather. However, starting with the GOES M spacecraft, expected to be launched in 2000, all will carry an SXI to observe solar flares and other aspects of "space weather".

A major issue addressed in this study is the choice of the stereo viewing angle, equivalent to the SXCI spacecraft-Sun-Earth angle. We considered both slightly elliptic "drifting" orbits and circular fixed-angle orbits. For either type of orbit, the SXCI spacecraft is initially placed in a slightly elliptical ~1 AU orbit; the spacecraft then separates ("drifts") from Earth at a rate determined by the ellipticity of the orbit. If a fixed-angle 1 AU orbit is desired, when the spacecraft reaches that angle, a spacecraft engine burn is necessary to circularize the orbit. Thus, a fixed angle orbit is inherently more expensive because the necessary propulsion system and fuel for the circularization maneuver must be included in the payload, and this significantly increases the mass and cost.

The spacecraft plus instrument dry mass basedlined in this study was 129 kg. A Pegasus XL could be used to place the spacecraft in Earth orbit and a solid rocket motor then injects it into the ~1 AU drifting heliocentric orbit. The spacecraft cost was estimated to be $17.3M. A study of the impact on the spacecraft and launch vehicle showed that the increase in spacecraft mass in low Earth orbit required for later orbit circularization would require use of a higher performance launch vehicle such as the Lockheed-Martin Athena I or Orbital Science Corporation Taurus XL instead of the cheaper Pegasus XL. This change in launch vehicle alone would increases the total mission cost by about $9M.

The optimum stereo angle for data analysis is not yet known (see Sec. 3) and it may well vary with the size or type of coronal feature. Therefore, based on both cost and scientific considerations, we concluded that a drifting orbit sampling a wide range of angles is best for the first stereo X-ray mission. In the final orbit chosen for the study, the spacecraft drifts away from the Earth in a slightly elliptical (0.9 AU periapsis x 1.0 AU apoapsis) heliocentric orbit. As shown in Fig. 3, a stereo angle of 25° degrees is achieved 260 days after launch and remains constant (± 1°) for 160 days. This provides a stable observing environment for the collection of stereoscopic images and occurs because of the phasing of the nearly identical orbits of the Earth and spacecraft about the Sun. No additional propulsive maneuvers are needed after the initial injection into heliocentric orbit. The dwells at ~25° and ~51° seen in Fig. 3 result from the varying orbital velocity of the elliptical spacecraft orbit. The baseline mission costed in Sec. 9 ends at 420 days. However, if the mission is extended, the new science objectives described in Table I can be addressed when the angle is >40°.

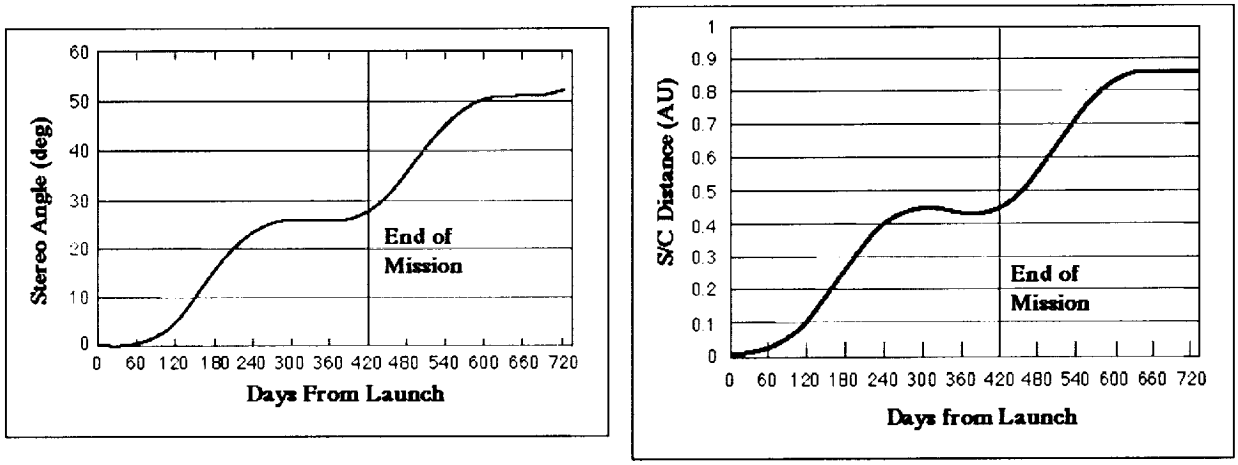

Fig. 3: Left: Stereo (Earth-Sun-S/C) Angle vs. Flight Time shows S/C dwells near 25° stereo angle. Right: Spacecraft distance from Earth vs. flight time.

6. THE SOFT X-RAY IMAGING (SXI) INSTRUMENT

The Skylab and Yohkoh missions carried grazing incidence soft X-ray telescopes to image the characteristic emission of the high temperature ionized gas of which the corona is composed. In addition to revolutionizing our view of the corona, these missions demonstrated how coronal images could be used to identify and locate the sites of activity which are responsible for ejecting the particles and fields into interplanetary space which frequently disrupt the terrestrial system. From these observations, NOAA concluded that access to coronal X-ray images on a continuous basis would vastly improve their ability to forecast "space weather." The SXIs that will be included in the complement of instruments to be flown on all future GOES satellites, starting with GOES M, are the outcome of this conclusion. The first SXI, developed at MSFC for GOES M, was and is viewed as a pathfinder and because it is an add-on to an existing spacecraft its design is severely constrained by the envelope available in the stowed (launch) configuration. The later GOES spacecraft will fly improved versions of the SXI instruments incorporating an advanced detector which will improve their imaging performance. The improved SXIs for

GOES N, O, P, and Q will be build by Lockheed Martin, Palo Alto (selected in June 1997 under a competitive GSFC procurement).

The first GOES M SXI telescope consists of a grazing incidence mirror, a twelve position broadband filter wheel and a focal plane assembly containing an intensified CCD camera with 5 arcsec pixels. The mirror consists of standard paraboloid hyperboloid reflecting surfaces in a Wolter I configuration fabricated from a single zerodur element. Spectral information is obtained using a 12-position filter wheel which contains 9 analysis filters which form two groups of short and long wavelength broadband filters. The temperature of the emitting region is found from the ratio of the emission using one long wavelength and one short wavelength filter. The SXI will be able to image density structures with temperatures in the range 1-10 MK. Although the solar corona contains material across the full temperature range, the brightest features are generally the hottest and their spectra are biased toward higher energy (shorter wavelength) photons. Standard, front illuminated, CCDs are also more sensitive to the higher energy photons in this range, which amplifies this effect and makes it difficult to resolve the cooler structures. Therefore, since one of the objectives of the SXI program was to observe coronal hole boundaries, which are relatively weak features, front illuminated CCDs were rejected in favor of an intensified CCD, i.e., a combination of a microchannel plate (MCP), phosphor coated coupler and a CCD in order to enhance the sensitivity to cooler features. Since the sensitivity of an MCP is inversely proportional to energy, i.e., it is more sensitive at longer wavelengths, it acts to reduce, rather than amplify, the intrinsic dynamic range in each image.

The GOES N through Q SXI instruments will benefit from recent technological developments in CCD manufacturing and will have an improved detector in the form of a mechanically shuttered, directly illuminated CCD. A contract for the GOES N through Q instruments has been placed by the GOES Project Office with Lockheed Martin and the first improved SXI should be in orbit circa 2001. Consequently we have chosen to baseline the SXCI mission using improved SXIs for both elements of the stereo pair, i.e. the Earth orbiting and the interplanetary telescopes. If it is decided to proceed with the SXCI program, the interplanetary instrument could be fabricated alongside the GOES SXIs since the design requirements for instruments flying in geosynchronous or interplanetary orbits are very similar. Such an approach would enable the SXCI telescope to be acquired at a competitive price, estimated to be in the range of $12-14M.

7. SPACECRAFT AND LAUNCH VEHICLE

The SXCI spacecraft concept developed for this study minimizes cost and risk by using a combination of design simplicity, extensive design heritage, and generous performance margins. Figure 4 shows front and back views of the spacecraft external arrangement in its post-injection configuration. The spacecraft is approximately 1150 mm (45.3") in diameter by 2131 mm (84.0") high. It weighs about 129 kg after injection when the solid rocket motor propellant has been depleted. We have selected the Pegasus XL launch vehicle for SXCI because of its combination of throw weight performance and fairing envelope, which simplifies packaging of the spacecraft. Fig. 5 shows a side view of the SXCI spacecraft integrated inside the enhanced Pegasus XL fairing envelope.

Placehold figures only!!!!!TO be replace by S/C figures

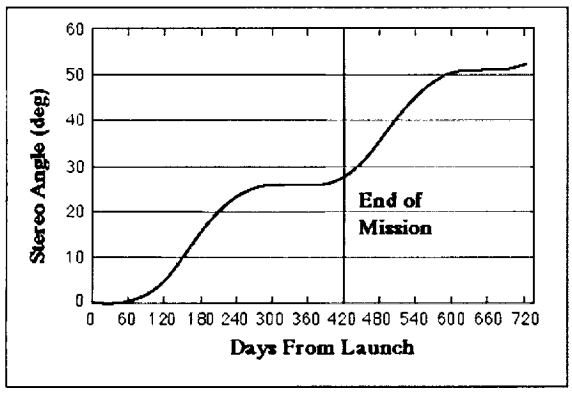

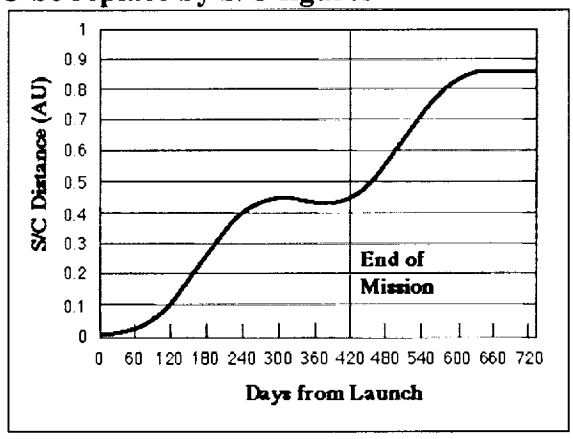

Fig. 4 (old 7-1_: SXCI Spacecraft **Fig.5 (old 7-7)**

A cylindrical solar array ensures adequate power generation during all mission phases and Sun angles and during the downlinks (Fig. 4). This design approach was chosen to avoid the need to deploy or articulate the array. The medium gain antenna is mounted below the array using a short mast. A flat cylindrical sunshield/radiator is mounted above the array. The

SXCI payload (the X-ray telescope) is mounted on the equipment deck inside the sunshield to allow a clear view of the Sun (through the aperture in the sunshield/radiator) and to provide a clear radiator field of view for focal plane cooling. The 608x608 mm (24.0x24.0") diameter high gain antenna (HGA) array is mounted to the top of the sunshield/radiator. The antenna is fixed, so the spacecraft rotates to turn the antenna towards Earth for communications. The nozzle of the Star-27 G solid rocket motor can be seen beneath the bottom edge of the solar array in Fig. 4.

The Deep Space Network 34 meter antennas are used to communicate with the spacecraft, using X band frequencies. The downlink from the spacecraft contains science data as well as engineering, instrument, and navigation data. The data rate during the prime mission phase (at 0.45 AU) is 70 kbps. Our design approach uses low, medium and high gain antennas, a Small Deep-Space Transponder and a 22W TWTA X-band power amplifier.

8. MISSION OPERATIONS AND COST

8.1 Data and observation strategies for maximum science return

Since this is a deep-space imaging mission, data return and telemetry are major issues. In addition to the usual data compression strategies used in imaging missions, the SXCI mission can use a unique new strategy for maximizing the science return by taking advantage of the simultaneous observations of the Sun from the Earth-orbiting GOES telescope. The basic concept is to store much more imaging data on board than can be downlinked; data from periods of interest as determined from the GOES data are then selectively downlinked. To implement this strategy, we sized the on-board memory at 22 Gbits. This does not cause a large mass or cost penalty because 10-20 Gbit erasable disk mass memory devices weighing about 5 kg are now available for about $500K. The memory has been sized to accommodate several days of data. A normal full disk image requires 12 bits per pixel and is composed of 512x512 pixels for 3 Mbits per image. Hence, the on board disk can hold approximately 7000 full disk images before it begins to overwrite itself. Data would be recorded at a much higher cadence than 1 Gbit per day. Specifically, data could be recorded at a high enough cadence to observe the complete evolution of CMEs and flares. Scientists would monitor the GOES and other near-Earth observations daily and determine which portions of the data should be downlinked and which portions should be marked for deletion. This information is uplinked to the spacecraft during the scheduled uplink/downlink periods. Since the data can remain on the recorder for several days before being downlinked, this strategy can be implemented within a low cost 40-hour/week mission operations schedule with several downlink periods per week. Only with both the large on-board storage and the knowledge of the event times from near-Earth observations is this strategy made possible.

The data rate during the prime mission phase (~0.45 AU from Earth) is approximately 70 kbps. We estimate that about 720 hours of 34m Deep Space Network (DSN) time would be used to cover the entire mission. During the prime science phase (23 weeks), the spacecraft could downlink data 3 times a weeks for a total weekly data volume of about 5 Gbits (~1700 images/week) and a total prime phase volume of 120 Gbits or 39,000 images. The total data volume from the mid-course phase would be 49 Gbits or 16,000 images assuming 182 hours of DSN time for this phase.

8.2 Ground system

The ground system baselined for this mission is based on the use of existing JPL Advanced Multi-Mission Operations System (AMMOS) capabilities, including hardware, software, and operations personnel. Because the SXCI spacecraft has only one science instrument (which is always Sun pointed except during downlinks) and a large onboard data storage capacity for flexibility, the ground system can be operated by an 8-person team working normal business hour, keeping operations costs low.

8.3 Mission cost

A first-order cost estimate was produced using a combination of grassroots and analogy methods, according to assumptions and guidelines specified in the SMEX Announcement of Opportunity issued April, 1997. These include a cost for DSN time of $1.6K/hour. The total mission cost was estimated to be $78.4M in $FY97 assuming a launch in September 2000. The cost breakdown for Phases A-D and E is shown in Table III. Additional costs included in the total the $19M cost of the launch (vehicle and services) and $2.9M for ground system development.

Table III. Cost Breakdown for Phases A/B/C/D and Phase E

	A/B/C/D	E
Project Management	1.6	0.6

Science	1.8	10.0
Outreach	0.4	1.2
Operations & Mission Design	0.7	2.6
Spacecraft (includes JPL overhead on subcontract)	18.3	0
Instrument (includes JPL overhead on subcontract)	14.0	0
Reserves	5.4	0
TOTAL (Phases A/B/C/D)	42.2	14.4

9. ACKNOWLEDGMENTS

This study was support by NASA's Offices of Advanced Technology & Mission Studies and Information System. A portion of this work was carried out at the Jet Propulsion Laboratory, California Institute of Technology, under a contract with NASA. We would like to thank Jeffrey R. Hall, David J. Freda, Jean J. Lorre and Shigeru Suzuki, JPL, for their contributions to the advanced visualization and analysis portion of this study and Gregory J. Garner and Aron A. Wolf, JPL, for their contributions to the mission design and cost portion this study. We would also like to acknowledge help and support from several scientists during this study including Joe Davila, Bruce Goldstein, Joe Gurman, Joan Feyman, Marcia Neugebauer, David Rust, and Dennis Socker.

10. REFERENCES

1. McClymont, A. N., Jiao, L, and Mikic, A., (1997) "Problems and Progress in Computing three-dimensional coronal active region magnetic fields from boundary data," *Solar Phys.*, 174, 191.
2. Alexander, D. and Katsev, S., 1996, *Solar Phys.*, 153, 153
3. Forbes, T. G., and Acton, L. W. 1996, *Astrophys. J*, 459, 330
4. Mikic, Z. and Linker, J. A., 1994, *Astrophys. J*, 430, 898.
5. Isenberg, P.A., Forbes, T.G., and Demoulin, P., 1993, *Astrophys. J.*, 417, 368.
6. Feynman, J., and. Martin, S. F.: 1995, *J. Geophys Res.*, 100, 3355.
7. Antiochos, S. K., 1997, "Theories of Coronal Mass Ejections," *EOS* 78, Vol. 78, No. 46 Supplement, F575.
8. Pevtsov, A., Canfield, R. C., and Zirin, H., 1996, *Astrophys. J*, 473, 533.
9. Rust, D. M. and Kumar, A., 1994, *Astrophys. J*, 464,L199.
10. Moore, R. L, Schmieder, B., Hathaway, D. H., and Tarbell, T. D., 1997,"3-D Magnetic Field Configuration Late in a Large Two-Ribbon Flare." (MSFC Report).
11. Berton, R., and Sakurai, T., 1985, *Solar Phys.*, 96, 93.
12. Gary, G. A., Davis, J. M., and Moore, R.: 1997, *Solar Phys.* "Comments On Solar Stereographic Missions For The Analysis Of Coronal Plasma Structures" (in press).
13. Lorre, J. J., De Jong, E. M., Ingersol, A., 1997 (private communication).